Journal of Rehabilitation in Civil Engineering 13-4 (2025) 207-228

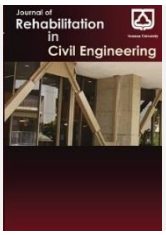

Journal of Rehabilitation in Civil Engineering

Journal homepage: https://civiljournal.semnan.ac.ir/

Numerical Investigation of Seismic Performance of Steel Concentrically Braced Frames Subjected to Critical Consecutive Earthquakes

Sahar Rouzrokh [1]; Elham Rajabi [2]; Gholamreza Ghodrati Amiri [3*]

1. M.Sc. Student, Natural Disasters Prevention Research Center, School of Civil Engineering, Iran University of Science & Technology, Tehran, Iran
2. Assistant Professor, Qualitative and Quantitative Analysis of Fluids and Environmental Research Group, Department of Civil Engineering, Tafresh University, 39518-79611 Tafresh, Iran
3. Professor, Natural Disasters Prevention Research Center, School of Civil Engineering, Iran University of Science & Technology, Tehran, Iran
* Corresponding author: *ghodrati@iust.ac.ir*

ARTICLE INFO

Article history:
Received: 12 October 2024
Revised: 14 November 2024
Accepted: 14 January 2025

Keywords:
Critical successive earthquakes;
Seismic demand parameters;
Ideal artificial neural networks;
Empirical equation;
Damage index.

ABSTRACT

This paper evaluates the effect of critical successive-shocks on the seismic performance of steel concentrically braced frames (CBFs) for significant structural design parameters such as behavior factor(R), displacement amplification factor (Cd), maximum drift and damage index (DI). For this purpose, three CBFs with 3,7and 11-stories are investigated using IDA, nonlinear dynamic analysis (NDA) under recorded critical seismic scenarios with/without successive-shocks and pushover. Results show that the average of R-factors has a 14% reduction rate under successive earthquakes compared with that of individual earthquakes. While Cd is not significantly affected by successive shocks, the occurrence of secondary-shocks increased DI by 1.8 times. In severer cases, the maximum drift is increased by up to 2 times. Finally, the sensitivity of seismic demand parameters to periods, PGA of first and second-shock is also evaluated by training an ideal ANN and proposing the empirical equations. Moreover, the effect of artificial successive shocks is examined on the seismic performance of CBFs. Despite what is necessitated in the seismic design codes, considering a constant value as R-factor for the whole steel structure cannot lead to the proper design of these structures especially under successive scenarios. Also, the use of artificial consecutive earthquakes can cause the inadequate assessment of seismic performance.

E-ISSN: 2345-4423

How to cite this article:
Rouzrokh, S. , Rajabi, E. and Ghodrati Amiri, G. (2025). Numerical Investigation of Seismic Performance of Steel Concentrically Braced Frames Subjected to Critical Consecutive Earthquakes. Journal of Rehabilitation in Civil Engineering, 13(4), 207-228. https://doi.org/10.22075/jrce.2025.35507.2179

1. Introduction

In seismically active regions, strong ground motions consist of several shocks, and the main earthquakes are usually accompanied by foreshocks and aftershocks with considerable magnitude. The occurrence of several consecutive earthquakes with a short time interval in the same region is called the seismic sequence phenomenon. Due to the short time interval between the occurrence of two earthquakes, there is often no opportunity to repair and retrofit the structure. The damaged structure caused by the first shock will suffer more severe damages and even collapse under the next strong shocks. Nonetheless, most seismic design codes do not consider consecutive earthquakes, and all processes of the structural design are based on a single design earthquake.

Extensive damages caused by past earthquakes reveal the weaknesses of structural design methods based on existing seismic codes in estimating the suitable performance of buildings under sequence-type ground motions. For example, the 2015 Nepal earthquake (M_w =7.8) had a series of aftershocks with a time interval of a few minutes after the main earthquake. A strong aftershock (M_w=6.7) was reported immediately after the main earthquake, and the second strong aftershock (M_w =7.3) occurred about 17 days after the main-shock. The occurrence of subsequent earthquakes increased the casualties and damage of the structures that had suffered damage under the main earthquake [1]. The 2018 Taiwan earthquake (M_w =6.4) had 11 foreshocks with magnitudes greater than 4.6 and a series of aftershocks, the strongest of which was recorded to be 5.7. This recurrence of shocks led to structural damages and the collapse of some high-rise buildings. In recent years, many studies have been performed on consecutive earthquakes and their effect on the different responses of single degree of freedom (SDOF) and the multi-degree of freedom (MDOF) structures such as damage spectra [2–5], ductility demand [6–8] and displacement demand [9–11]. Some studies have emphasized the necessity of improving ductility by using new methods [12–17].

Several studies on the effects of consecutive earthquakes on the damage of structures showed that the repetition of earthquakes in seismic regions increases the damages, making recovery near impossible due to the short time intervals between the events [18]. The study of Ke et al. [4] found that the energy modification factor of steel frames equipped with SMAs under mainshock-aftershock earthquake sequences is higher than that under single mainshocks. Also, Shokrabadi [19] assessment of the economic loss of the structure during its service life under seismic sequence found that aftershocks can increase the losses by more than 30% compared with that of a single mainshock. Likewise, the investigations of Fang et al. [5] confirm that multiple earthquakes have a significant effect on various performances of the structures. For the maximum considered earthquake (MCE), the probabilities of collapse for structures with single-core and dual-core SCBs (structures S-SCF and D-SCF) increase from 18% to 28% and from 10% to 16%, respectively with considering the aftershocks [5].

Recent evaluation of BRB frames under consecutive earthquakes indicates that seismic sequence has increased the overall global ductility factor, story drift, and residual drift of BRB frames [7]. Time history analysis for a reinforced concrete structure under five consecutive earthquakes showed that a structure under seismic sequence has an average of 26% and 37% increase in horizontal displacement and drift, respectively [11]. The numerous literatures present on changes in the behavior factor (R factor) of different structures under successive earthquakes show the importance of this parameter in the seismic design criteria of structures and their inelastic performance. During an earthquake, structures typically undergo deformations and stresses beyond the elastic limit, causing the large and unrealistic strengths. As a result, it requires the design of sections with large

and non-economic dimensions. Hence, the elastic lateral force is decreased by the behavior factor parameter, which depends on ductility, over-strength, damping, and etc. Generally, a structure absorbs a large amount of seismic energy by inelastic deformations. Therefore, structures are designed with a lesser force than the amount caused by elastic behavior. Moreover, damage estimation in structures can be effective in crisis management. Studies on SDOF and MDOF structures indicate that aftershocks and earthquake recurrences have led to a reduction in the behavior factor of structures [20–23].

The studies of Abdollahzadeh et al. [24] on the effect of earthquake recurrence on the behavior factor of steel moment frames showed that the behavior factor decreased under successive earthquakes. Although the importance of seismic sequence phenomenon on seismic demand parameters has been studied in engineering literature, much research is still needed on building performance, variation of seismic demand parameters for different lateral force resisting systems against critical successive ground motions and on expanding the results to meet a wide range of structures using machine learning, such as neural networks. For this purpose, effective factors in the structural design procedure and damage distribution need to be evaluated and considered as recorded consecutive seismic scenarios. In this regard, the R factors, C_d coefficients, damage distribution and maximum drift of steel concentrically braced frames (CBFs) are calculated by considering the critical seismic sequence phenomenon and compared for artificial successive records. Three 2D special concentrically braced frames (chevron-braced frames) with 3, 7, and 11 stories are designed according to the Iranian earthquake design code standard No. 2800, Fourth Edition and implemented in the Opensees (Open System for Earthquake Engineering Simulation) software as a powerful software for the nonlinear structures analysis. The critical successive ground motions records are initially used in the present paper due to the inaccuracy of the artificial seismic sequence simulation methods. Because the evaluation of the R factors, C_d coefficients, damage distribution and maximum drift of CBFs under successive earthquakes requires time-consuming analyses and the number of studied CBFs is limited, the variation of these parameters is evaluated by an ideal artificial neural network. In this regard, results of IDA, NDA and pushover is used for designing the ideal network so that this network is well able to estimate the desired results of CBFs based on the structural properties and characteristics of consecutive earthquakes. Moreover, the sensitivity of the seismic demand parameters and structural damage to different parameters can also be performed using trained ANN for recorded and artificial successive records. Examination of results under selected ground motion records – with/without sequence, recorded/artificial – show that the seismic demand parameters and damage index are significantly affected by the seismic sequence phenomenon, and the use of a single design earthquake causes an unrealistic behavior in the structure, leading to early on building collapses before than what is often assumed in the seismic design codes. Moreover, artificial successive earthquakes result in the non-conservative performance of structures. Finally, empirical equations are proposed based on ideal ANN for more comprehensive examination of the desired parameters. Fig 1 shows the research methodology of this study.

2. Critical successive earthquakes

This paper focuses on the seismic demand parameters and structural damage evaluation of CBFs under critical mainshock-aftershock sequences. For this purpose, the critical seismic scenarios - with/without sequence, of which the designer obtains the maximum response-, are selected based on the EPA suggested by Amiri and Manouchehri Dana [25].

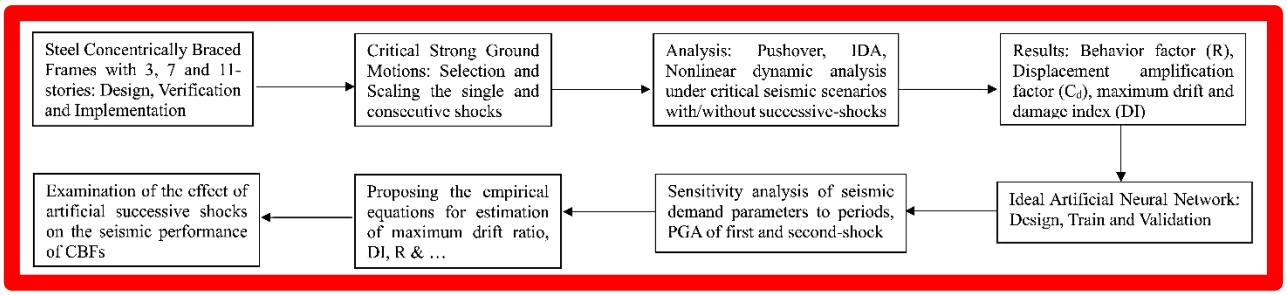

Fig. 1. The research methodology of this study.

The parameter EPA is the mean value for the acceleration response spectrum (for 5% damping) for periods between 0.1 and 0.5 s divided by a standard amplification coefficient of 2.5. Moreover, this parameter includes the frequency content of earthquakes. In this regard, 15 real seismic sequences containing main-shock with foreshocks or aftershocks are obtained from the Pacific Earthquake Engineering Research Center (PEER). For critical successive scenarios, the first and second shocks were recorded at a maximum interval of ten days from each other at the same station and in the same direction and have the maximum EPA among the ground motions recorded for the same event by other stations. Also, a time gap of 100 (s) is considered between the first and second earthquakes. This gap is adequate to cease the building's motion due to the damping under the first event [26]. The features of the critical consecutive ground motion records used in this paper are presented in Table 1. It should be noted that the selected earthquakes are not only in the form of the mainshock-aftershock sequences, but also consecutive earthquakes such as foreshock-mainshock or two successive foreshocks, including the seismic sequence phenomenon.

Table 1. Characteristics of critical consecutive records.

Earthquake	Station	Date	Mw	PGA (g)	EPA (g)
Chalfant Valley	CDMG 54428 Zack Brothers Ranch	7/20/1986 14:29	5.77	0.238	0.245
		7/21/1986 14:51	5.65	0.135	0.105
	CDMG 54214 Long Valley Dam (Upr L Abut)	5/25/1980 16:49	5.69	0.137	0.088
		5/25/1980 20:35	5.70	0.240	0.216
		5/25/1980 20:35	5.70	0.240	0.216
		5/27/1980 14:51	5.94	0.629	0.429
Mammoth Lakes	CDMG 54099 Convict Creek	5/26/1980 18:58	5.70	0.093	0.112
		5/27/1980 14:51	5.94	0.629	0.429
		5/25/1980 19:44	5.91	0.217	0.204
		5/27/1980 14:51	5.94	0.317	0.221
		5/26/1980 18:58	5.70	0.123	0.091
	USGS 43 Fish & Game (FIS)	5/27/1980 14:51	5.94	0.317	0.221
		5/27/1980 19:01	4.73	0.100	0.078
		5/31/1980 15:16	4.80	0.190	0.187
Northwest	CSB 19001 Jiashi	4/5/1997 23:46	5.90	0.244	0.188
		4/11/1997 05:34	6.10	0.296	0.228
	CSB 19002 Xiker	4/5/1997 23:46	5.90	0.039	0.039
		4/15/1997 18:19	5.80	0.100	0.105
Kozani	ITSAK 99999 Grevena	5/15/1995 04:13	5.10	0.041	0.040
		5/17/1995 04:14	5.30	0.024	0.016
	ITSAK 99999 Chromio Anapsiktirio	5/15/1995 04:13	5.10	0.133	0.093
		5/17/1995 04:14	5.30	0.114	0.102
Chi- Chi	CWB 9999936 TCU129	9/20/1999 17:57	5.90	0.117	0.103
		9/20/1999 18:03	5.70	0.608	0.284
Coalinga	CDMG 47T03 Sulphur Baths (temp)	7/22/1983 03:43	4.89	0.040	0.025
		7/25/1983 22:31	5.21	0.205	0.101
	CDMG 46617 Coalinga-14th & Elm (Old CHP)	7/22/1983 03:43	4.89	0.154	0.099
		7/25/1983 22:31	5.21	0.581	0.351
Managua	3501 Managua, ESSO	12/23/1972 06:29	6.24	0.394	0.331
		12/23/1972 07:19	5.20	0.295	0.235

3. Steel concentrically braced frames

Since steel bracings are one of the most widely used systems for resisting transverse loads in the design and retrofit of concrete and steel structures[27][28], three 2D special chevron-braced frames with 3, 7, and 11 stories -the number of common stories in Iran- representing short, medium, and relatively high-rise structures are considered in this study. These frames are designed based on the Iranian earthquake design code standard No. 2800, fourth edition. The geometry of frames and specifications of the designed sections are illustrated in Fig 2 and Table 2. The height of the stories in all the frames is 3.2 m and includes a 5 m long three-bay. The frames are located in Iran's Tehran city with high seismic hazard, and the soil type C was assumed. The yield and ultimate strength of the steel used in each frame is 2.4×108 N/m^2 and 3.8×108 N/m^2. The modulus of elasticity and the Poisson's ratio are considered to be 1.999×1011 N/m^2 and 0.3. The dead and live loads for stories are 500 kg/m^2 and 200 kg/m^2, and for the roof are 300 kg/m^2 and 150 kg/m^2, respectively. Earthquake loading is applied according to standard No. 2800.

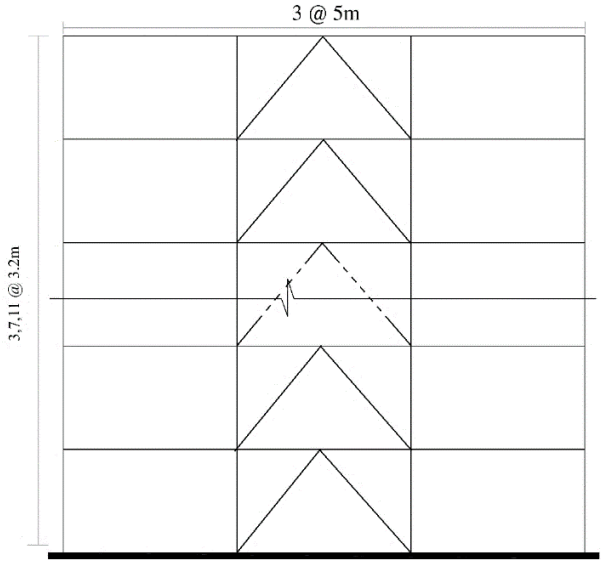

Fig. 2. Overview of studied concentrically braced frames.

Table 2. Geometric properties of the designed steel frames.

Frame	Story	Interior beams	Exterior beams	Interior columns	Exterior columns	Braces
3-story	1-2	IPE 600V	IPE 300	HE 240	HE 100	BOX 100*100*9
	3			HE 100	HE 100	BOX 90*90*8
7-story	1-2	IPE 600V	IPE 300	HE 500	HE 140	BOX 100*100*9
	3-4			HE 320	HE 120	BOX 100*100*9
	5-6			HE 240	HE 100	BOX 90*90*8
	7			HE 160	HE 100	BOX 90*90*8
11-story	1-2	IPE 600V	IPE 300	HE 700	HE 180	BOX 100*100*9
	3-4			HE 500	HE 180	BOX 100*100*9
	5-6-7			HE 360	HE 160	BOX 100*100*9
	8-9			HE 300	HE 140	BOX 100*100*9
	10			HE 300	HE 100	BOX 100*100*9
	11			HE 220	HE 100	BOX 90*90*8

All frames are designed and implemented in the finite element program of Opensees for nonlinear analyses. The inelastic behavior of the beam, column, and brace elements are modeled considering a distributed plasticity and plastic hinge with numerical integrations across the cross-sections and along the length of the member using fiber section nonlinear beam-column elements [29]. The

bilinear model of steel02 material with a strain hardening ratio equal to 2% on the strain stress diagram is assigned to all elements. The damping ratio is assumed to be 5% for each vibration mode in all frames. By applying mass as a combination of dead load in addition to 20% of the live load to the frame nodes and considering the elastic stiffness of the structure, the vibration period of the first mode of the structures is calculated, which in 3, 7, and 11 story frames are 0.27, 0.65 and 1.09 s, respectively. The results of Kim and Choi [30], which examined the behavior of chevron-braced frames, are used to verify the studied CBFs. For this purpose, the 9-story Chevron-braced frame with three bays - length is 6 meters - is re-modelled based on the selected elements and materials used in this research. After assigning the loading conditions and specifications of the used steel in [30], the first mode's frame vibration period is calculated. The period calculated by Kim and Choi [30] is 1.44 s, and the value obtained from the modelling process of the present paper is 1.46 s, which is a negligible and acceptable amount of difference.

4. Behavior factor

Behavior factor is an approximation of the ratio of seismic forces that the structure would experience if its response would be completely elastic to the seismic forces used for the design. In other words, the factor accounts for the capability of structures to exhibit ductile inelastic behavior connected with energy dissipation. In this study, R-factors are calculated based on [31], using the ductility and over-strength factors shown in Fig 3. In this regard, the maximum base shear for linear behaviour during an earthquake (V_e) requires the base shears of the first plastic hinge and maximum nonlinear base shear of the structure (V_s and V_y, respectively). As shown in Equation (1), due to the energy absorption and stored strength between the formations of the first plastic hinge (V_s) and the final yielding of the structure, the R factor depends on the reduction of linear V_e to maximum nonlinear V_y [31].

$$R = \frac{V_e}{V_y} \times \frac{V_y}{V_s} \tag{1}$$

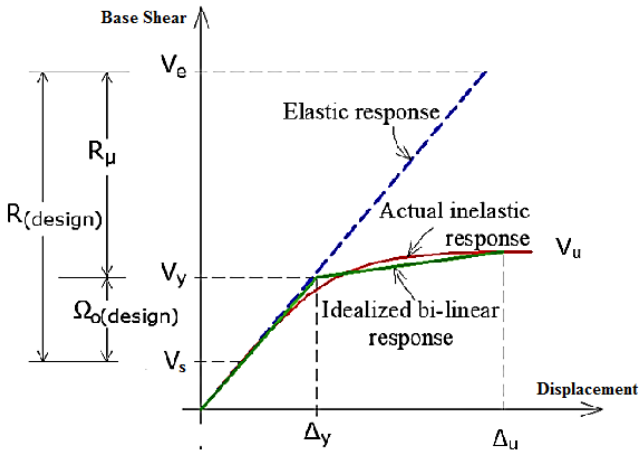

Fig. 3. Proposed force-displacement relationship in the Uang method [31].

5. Displacement amplification factor

Lateral displacement demand is one of the most important factors in performance-based design methods because many of the serious damages that occur during an earthquake are caused by lateral displacements in the structural and non-structural elements. Most structures endure the inelastic deformation in severe earthquakes. Therefore, reduction of the elastic seismic force demand is

permitted in modern seismic design code through a response modification factor. Since the structure design is based on reduced seismic force, the calculated displacements of elastic analysis need to be amplified to estimate more real deformations in severe earthquakes. The displacements that have been calculated through the seismic design code procedure are less than the maximum structural displacement during strong ground motions. In this regard, the maximum displacements or drifts of a structure in an earthquake are estimated based on Equation (2) by multiplying the displacement of the elastic analysis in the amplification factor (C_d). Therefore, the displacement amplification factor (C_d) is most widely employed for evaluating the inelastic performance of structures and is also used in the most common design procedures as a structural response parameter.

$$\Delta M = Cd \,.\, \Delta e \tag{2}$$

Where Δ_M is the inelastic displacement, Δ_e is the displacement calculated by elastic analysis, and C_d is the displacement amplification factor.

6. Damage index

The quantification of the structural damage due to excessive deformations or caused by the accumulated damage in earthquakes is an essential requirement in performance-based structural analysis. Damage indices have been widely used to predict possible damage through the ratio between the initial and the reduced resistance capacity of a structure. These indices have been formulated based on structural response of analytical evaluation such as hysteretic energy and maximum response, and typically normalizes the damage on a scale of 0 to 1, where zero represents the undamaged state, and unity represents collapse of the structure. Different damage indices are found in earthquake engineering literature. Park and Ang [32] used hysteretic energy and deformation to present a damage model based on Equation (3). This index is a combined seismic damage measure that integrates the damage caused by excessive deformations with the damage caused by the cumulative hysteretic energy dissipation [32]. Some researchers improved this simple index [33][34][35], but the Park-Ang model is still widely used in structural damage analysis [36][37].

$$DI = \frac{\delta_m}{\delta_u} + \frac{\beta}{P_y \delta_u} \int dE_{\not h} \tag{3}$$

Where δ_m is the maximum deformation of the element, δ_u is the ultimate deformation, β is a model constant parameter to control strength deterioration, $\int dE$ is the hysteresis energy absorbed by the element during the earthquake and P_y is the yield strength of the element. In order to calculate the Damage index – based on Equation (3) – β is taken as 0.025, according to Park et al. [32], for nominal strength deterioration in steel frames.

7. Artificial neural network (ANN)

Artificial neural networks are linear or nonlinear vector mappers between two specific spaces. This tool widely used in estimating the behavior/response of the structure [38][39][40]. Fig 4 shows that following the training of the neural networks, specific outputs are estimated by applying specific inputs. As long as the network output and the user's desired output (so-called target) match, the network is based on matching, and the symmetry adapts between the input and target. Multilayer feed-forward neural networks with a back-propagation error- algorithm (Fig. 4) are used in this

research to estimate the seismic demand parameters simultaneously in terms of R factors caused by successive earthquakes ($R_{sequence}$), maximum drift ratio for sequence to single state ($MD_{sequence/single}$) and damage index of successive earthquakes to single earthquakes ($DI_{sequence/single}$) for CBFs.

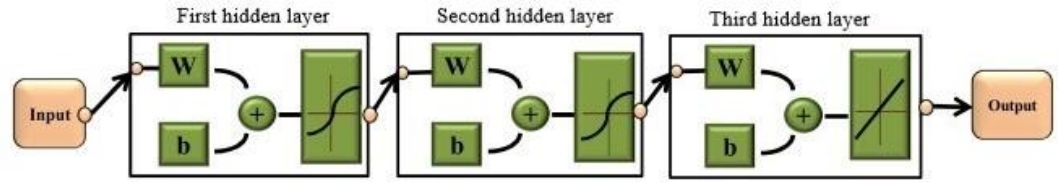

Fig. 4. An overview of the networks used in this study.

A back-propagation network, which is a multilayer network with a nonlinear transmission function, is designed using the Widrow -Hoff learning rule. This network uses the input and target vectors for training to approximate a function, find the relationship between input and output, and classify the neural network inputs. This network includes Bias, one or more sigmoid middle layers, and a linear output layer, and it can estimate any function with a limited number of discontinuity points. The standard back-propagation network is an algorithm with slope reduction, in which the network weights move in the opposite slope of the efficiency function. In this algorithm, first, it is assumed that the network weights are randomly selected. In each step, the network output is calculated, and according to the difference between the target and outputs, the weights are corrected to minimize the error. In the back-propagation algorithm, each neuron's excitation function is considered equal to the weighted sum of its inputs. The Lunberg-Marquardt method is used in the next step to communicate the error in the inputs, weights, and outputs. This is the standard method for least square problems and is a combination of the Newton Gaussian method and the maximum descent slope. This algorithm randomly divides the data into three parts: training, validation, and testing [41]. Here, the values of 60%, 35%, and 5% are randomly selected for training, testing, and validation, respectively, to obtain the most efficient distribution sets of data and prevent the over fitting issue. The criterion for stopping the training of networks is the mean squared error (MSE). So low MSE values mean better network performance, and zero values mean no errors. On the other hand, regression values (R) represent the degree of correlation between network outputs and the target. Thus, R=1 means complete correlation, and R=0 indicates randomness and no correlation. Therefore, two criteria, MSE and R, are selected to select the ideal neural network. Moreover, homogeneous information is essential to achieve a proper neural network model. In this regard, among the seismic properties, parameters such as the first and second earthquake PGA (PGA_m and PGA_a, respectively), magnitude of first shock (M_m), structural properties such as structure type and height, in the form of the vibration period (T) and target ID – equal to 1 for $R_{sequence}$, 2 for $DI_{sequence/single}$ and 3 for $MD_{sequence/single}$ for an estimation of 3 targets by one ANN – are selected as input and reduced behavior factor under consecutive occurrences of seismic scenarios ($R_{sequence}$), $DI_{sequence/single}$ and $MD_{sequence/single}$ -, the analytical results of sets of 3, 7 and 11-story frames - have been selected as the target values for training, testing, and verification of the artificial neural network. The statistical properties of inputs and targets are listed in Table 3.

Table 3. Statistical specifications of input parameters.

Input	T (s)	M_m	PGA_m	PGA_a	ID
Min	0.260	4.730	0.00073	0.00072	1
Max	1.087	6.240	0.8064	1.803	3
Mean	0.666	5.541	0.0844	0.2948	–

Moreover, the input(s) and target(s) are presented graphically in Fig 5. The periodicity parameter separates the results of the frames from each other. Also, to avoid over fitting, the optimum number of nodes in the hidden layers should be selected according to [41], as this number of nodes strongly affects the performance of the neural network. Smaller numbers will lead to the inability of the network to fit the data, and larger numbers will lead to over-fitting. As mentioned earlier, the neural networks consist of the sigmoid transmission function in hidden layers. This function always behaves between 0 and 1. Thus, before training the networks, it is necessary to normalize all data, including input and target values. In this regard, the linear interpolation method is used to scale the data between 0.1 and 0.9. After introducing the normalized input and target data to the network and training to minimize the amount of error, the desired output is extracted.

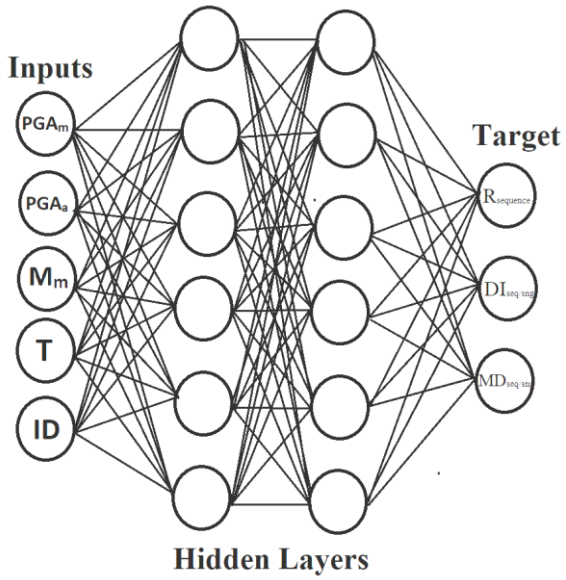

Fig. 5. Schematic view of inputs and targets.

6. Results of seismic demand parameters and damage

6.1. Behavior factors of CBFs under single and critical successive earthquakes

As mentioned in the previous sections, calculating the behavior factor parameters under the ground motion records requires nonlinear static analysis (pushover), nonlinear time history, and incremental dynamic analysis (IDA). This procedure is used by Rajabi and Ghodrati Amiri [23] for reinforced concrete frames. The nonlinear static analysis is performed on the frames according to the Uang over-strength factor. The base shear corresponds to nonlinear behavior initiation, and the formation of the first plastic hinge in the structures (V_s) is extracted. The final nonlinear base shears (V_y) are obtained by performing IDA analysis. In the IDA method, nonlinear dynamic analysis of the structure under one or more seismic ground motion records, each of which is scaled to different intensity levels, is conducted from the elasticity to the collapse stage [42].

To perform IDA analysis, first, the seismic Intensity Measure (IM) from a small value is scaled and applied to earthquake records to demonstrate the elastic behavior of the structural model at a certain level of seismic intensity to achieve the desired failure of the structure, with an appropriate algorithm and scale factor, and the time history analysis is conducted under these records. Then, at the end of each analysis step, the Damage Measure (DM) corresponding to its seismic intensity level is recorded, and the IDA curve of Intensity Measure versus the Damage Measure is plotted. To

consider the parameters of the vibration period and damping, the spectral acceleration (S_a (T_1, 5%)) and maximum peak inter-story drift (θ_{max}) are selected as the IM and DM in this paper, respectively. Since this paper is based on extracting the behavior factor for structures designed according to the Iranian earthquake design code standard No. 2800, the performance levels are determined using the definitions of this standard. Since all the criteria in this standard are based on the performance level of life safety (LS), the maximum peak inter-story drift of frames in this performance level is considered to be 0.025 times the height of the story in buildings up to 5 floors and 0.02 times of the height the story in other buildings. The seismic standard No. 2800 does not provide a criterion for collapse prevention performance (CP). As a result, the maximum peak inter-story drift at a complete structural damage state of 0.0533 for 3 and 7-story frames and 0.04 for the 11-story frame is considered in this paper and based on Table 5.9a 5.4.3.4 of the Hazus-MHM MR5 [43], Therefore, while all the IDA analyses are performed up to the CP performance level, the required seismic parameters such as the spectral acceleration and final nonlinear base shear (V_y) are obtained at the LS performance level. According to the Uang ductility factor, the maximum linear base shear of the structure (V_e) is calculated by performing the time history dynamic analysis assuming the elastic behavior of the members of the structures. It should be noted that all frames are subjected to gravity loading before performing other analyses. The pushover analysis with the lateral load pattern related to the first mode is performed on the frames according to standard No.2800. Base shears corresponding to the initiation of inelastic behavior (V_s) are extracted for each frame. Fig 6 shows the pushover curve of 3, 7 and 11-story frames. IDA curves were obtained for 3, 7, and 11-story frames under 15 critical earthquake records, with and without seismic sequences, by performing incremental dynamic analysis.

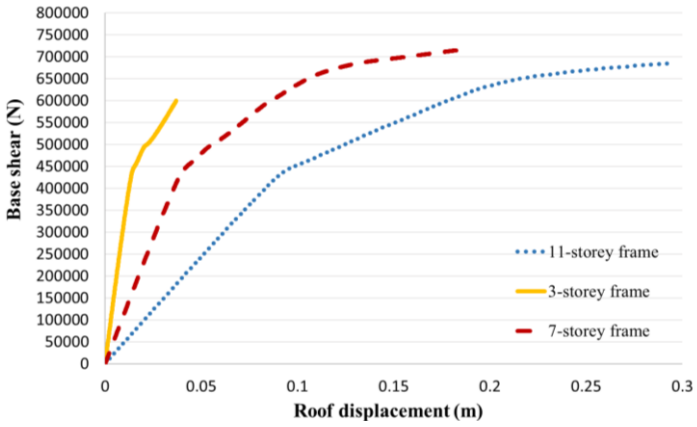

Fig. 6. Pushover curves of the studied CBFs.

To conduct IDA analysis under critical successive seismic scenarios, the first scaled earthquake causes a certain level of failure in the structure. After the considered time gap of 100 s, incremental dynamic analysis using the second scaled earthquake is performed until the structure collapsed. It should be noted that to calculate the desired scale factor, the spectrum of the main seismic record (with higher EPA value than others) is used as a criterion. The resulting scale factor is applied to critical successive seismic records and both the first and second seismic records are scaled together. As an example, Fig. 7 shows the IDA curves of the 3-story frame under single and critical successive earthquake records. Also, for better comparison, the average of IDA curves of all frames under the mentioned records is shown in Fig 8. As seen in the figure, the collapse capacity of the structure is decreased due to an increase in the damage level caused by the first earthquake. This is due to the accumulation of damage and increased damage to the frame elements caused by stiffness and strength deterioration. As a result, the 3, 7, and 11-story frames, which reached the desired

performance level and the corresponding maximum peak inter-story drift under a specific acceleration in the first earthquake, will reach the same performance level and maximum peak inter-story drift at a lower acceleration under the second earthquake.

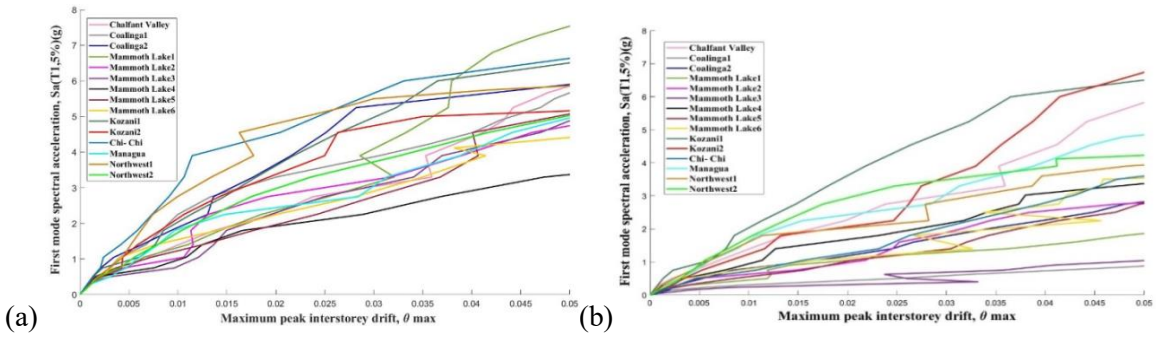

Fig. 7. IDA curves of the 3-story frame (a) under single critical earthquakes, (b) under critical successive earthquakes.

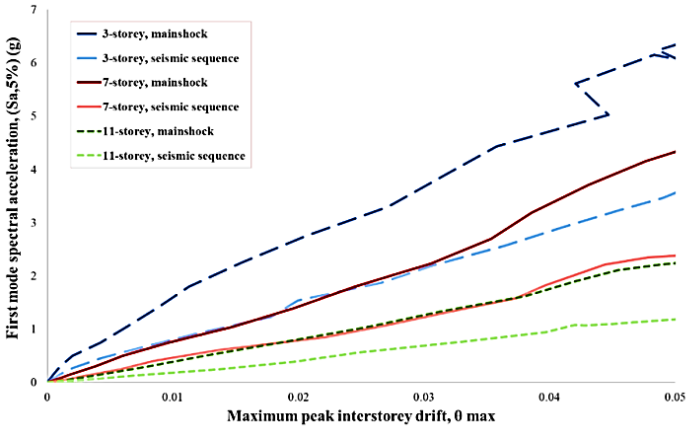

Fig. 8. Mean of IDA curves in 3, 7 and 11-story frames under single and critical successive earthquakes.

This means that the structure collapses much earlier in the face of subsequent earthquakes than in a single earthquake. The decrease in the capacity of the structure corresponding to the level of life safety performance is seen in Figs 7 and 8. Also, the IDA curves in Fig 8 show that increasing the height of the frames and decreasing the stiffness of the members places the structures in the nonlinear area and decreases the IM values in the diagrams for a constant value of DM. In other words, as the number of stories increases, the spectral acceleration of the first mode of the structure for an identical maximum peak inter-story drift decrease. The behaviour factors for CBFs are calculated according to the results of the nonlinear static and dynamic analyses under selected earthquake records. The results for each frame and the average of behavior factors are shown in Fig 9. The diagrams illustrate that the average of behavior factors of frames under critical successive earthquakes is reduced compared with that of single earthquakes. As seen in Fig 10, the behavior factor in the 3, 7 and 11-story frames is decreased by about 13%, 6%, and 22%, respectively.

Also, the average of behavior factors under the critical seismic sequence compared with the single seismic state shows a relative decrease of 14% in the total frames, which is due mainly to the increases in the damage level caused by the first critical earthquake. Furthermore, the structural members' capacity is decreased due to critical successive earthquakes. As a result, members can tolerate a lesser axial force than before, and the linear and nonlinear base shears and subsequently R-factor of the structure is reduced. Fig. 9 shows that the behavior factor does not change in any of

the frames because the first shock is predominant in both IDA analyses under records containing single and consecutive earthquakes. Under the successive earthquakes and at the same amount of spectral acceleration of the first earthquake, the structure reaches the maximum peak inter-story drift and follows maximum linear and nonlinear base shears, which yields identical results and, consequently, no change in the behavior factor.

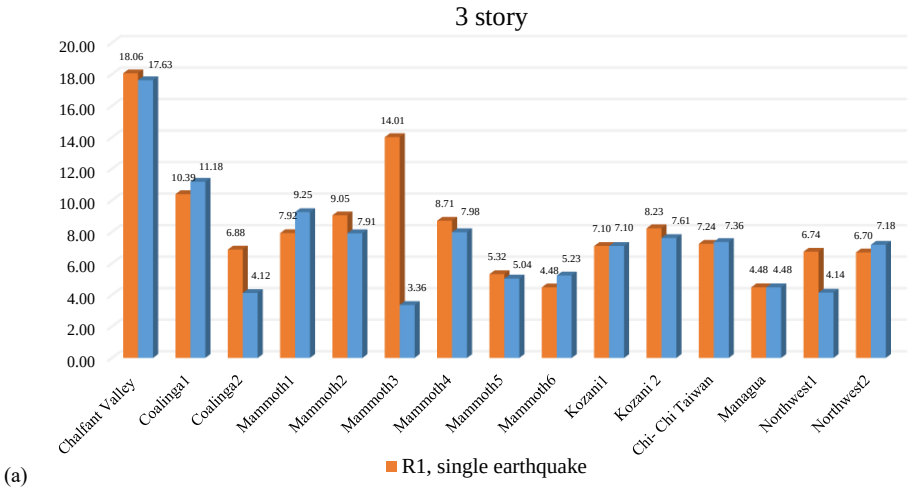

(a)

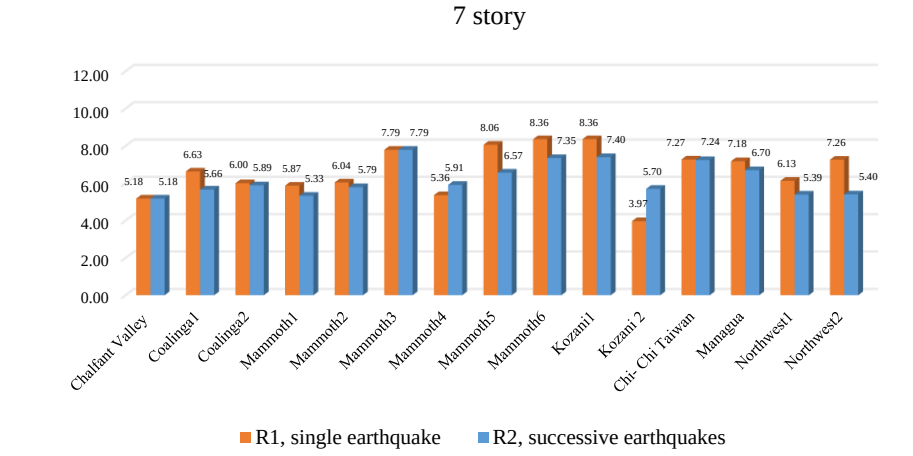

(b)

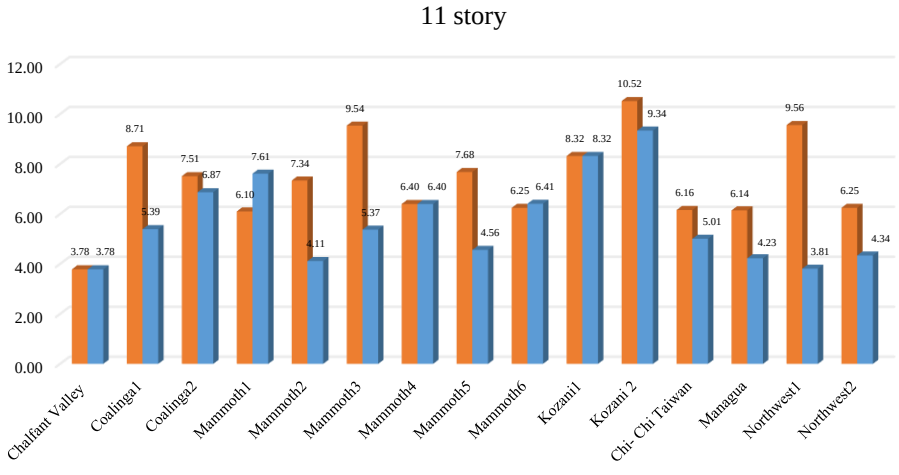

(c)

Fig. 9. Behavior factors of CBFs under single and critical successive earthquakes.

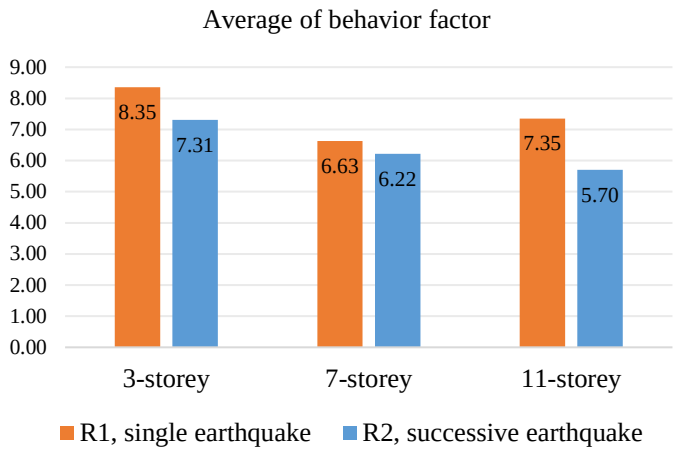

Fig. 10. Average of behavior factors of 3, 7 and 11-story frames under single and critical successive earthquakes.

Also, according to some records, the maximum linear base shear and behavior factor in all three frames is increased due to the proximity of the structure's dominant frequency to the predominant frequency range of the relevant earthquake and the resonance phenomenon. For example, in Fig 10, the behavior factor of the 3 and 11-story frames are decreased by about 0.76% and 0.44%, respectively, under consecutive Mammoth Lake3 earthquakes. But, in the 7-story frame, the behavior factor did not change under this record, and the amount of spectral acceleration corresponding to the desired displacement decreased significantly compared with that of the single earthquake. Therefore, the linear base shear of the structure under this amount of spectral acceleration is expected to decrease. Contrary to expectations, under consecutive earthquakes, the maximum linear base shear and the behavior factor are increased to the extent that the behavior factor in both single seismic and sequential seismic states are the same and do not change. As observed in Fig 11, the Fourier spectrum of the Mammoth Lake3 consecutive earthquakes record is richer in frequencies between 1.4 and 2.7 Hz, and the dominant frequency of the 7-story frame with a value of 1.54 Hz is also within this range, thus affecting the response of the structure. As a result, the maximum linear base shear and behavior factor of the structure is increased. As observed, the different heights and frequencies of the frames, the random nature of the earthquakes, and the difference in the earthquake records' frequency content led to behavioral differences in the record of each structure. For example, the behavior factor in one frame is constant, increased, or decreased under some records, while it is different in other frames under the same records. Therefore, the average result is used to judge the seismic sequence phenomenon's effect. The average index can use the data more thoroughly and value each result equally, while other statistical measurements such as mode and median do not lead to the same result between the three frames.

6.2. Damage index of CBFs under single and critical successive earthquakes

In this paper, structural damage of CBFs with 3, 7 and 11 stories are calculated using the Park and Ang damage index [32], presented in Equation (3). For this purpose, in addition to the result of the nonlinear static analysis, nonlinear dynamic analysis is performed for all CBFs under 15 critical single and successive earthquakes, which have been scaled according to the design spectrum of Standard No. 2800 using linear scaling [44] so to have identical spectral acceleration with the design spectrum of the fundamental period of each CBF. This technique is convenient for implementation, and the frequency content and original phasing of the records are also preserved in this method [44]. The ratio of the damage index caused by critical successive earthquakes to single

scenarios ($DI_{sequence/single}$) is shown in Fig. 12 for CBFs with 3, 7 and 11 stories. As shown in this figure, this ratio is greater than the one in most cases. This means that CBFs undergo more structural damage due to damage accumulation caused by first shocks. Fig. 13 shows the average of $DI_{sequence/single}$ for CBFs. The last bar in this figure presented the average of all ratios. The damage index is increased by 1.8 times due to occurrence of secondary shocks.

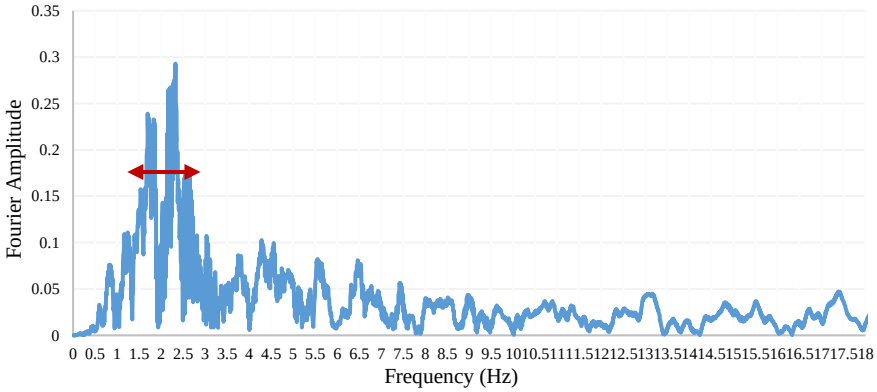

Fig. 11. Fourier spectrum acceleration of consecutive Mammoth Lake3 earthquake.

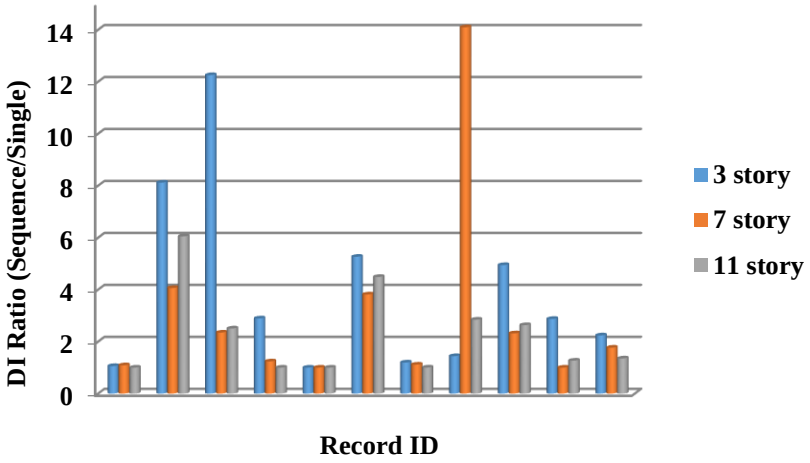

Fig. 12. Ratio of damage index caused by critical successive earthquakes to single scenarios.

6.3. Displacement amplification factor of CBFs under single and critical successive earthquakes

This section presents the results of C_d coefficients for all CBFs under seismic scenarios with and without sequence. For this purpose, inelastic drifts of CBFs which are calculated by nonlinear dynamic analyses divided into elastic drifts from linear analyses. This coefficient is determined for single and successive earthquakes and compared in Fig. 14 for some severe successive to single states. In most cases, CBFs undergo more drifts after second shocks, and C_d is increased in comparison with single shocks. If the C_d ratio is equal to one, the first shock is considered stronger and more severe than the second shock. The average of the C_d ratio for the studied frames is shown in Fig 15. In general, the C_d coefficient is not significantly affected by all selected successive shocks. Variation of the maximum roof drift for the studied CBFs under several critical consecutive scenarios as opposed to single earthquakes is presented in Fig 16. These ratios are not significantly high, except in several states in which the dynamic properties of the CBFs are probably closer to seismic scenarios.

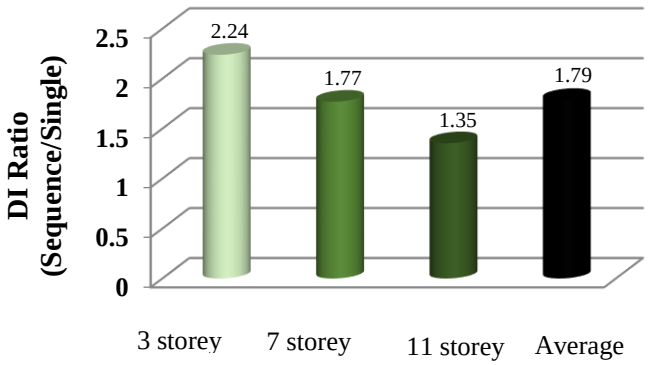

Fig. 13. Average ratio of damage index caused by critical successive earthquakes to single scenarios.

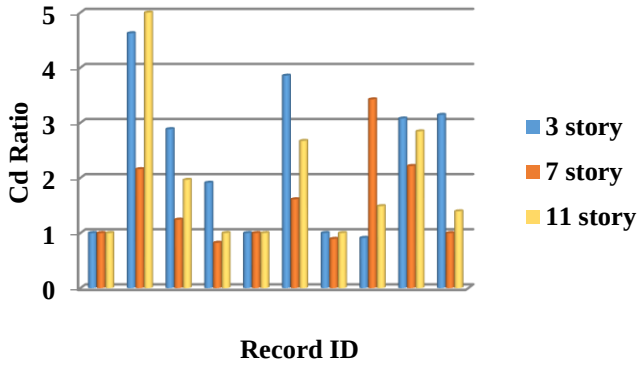

Fig. 14. C_d ratios for CBFs with 3, 7 and 11 story.

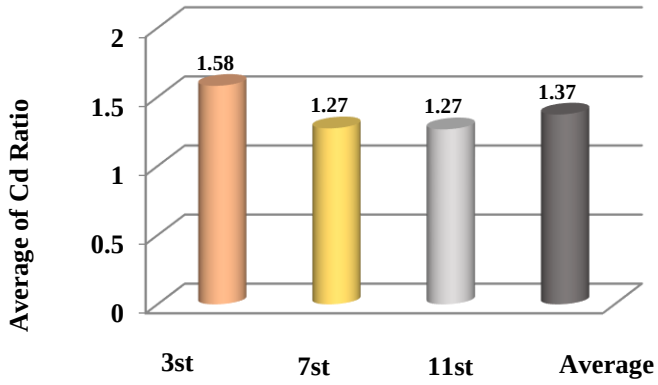

Fig. 15. Average of C_d ratios for CBFs with 3, 7 and 11 story.

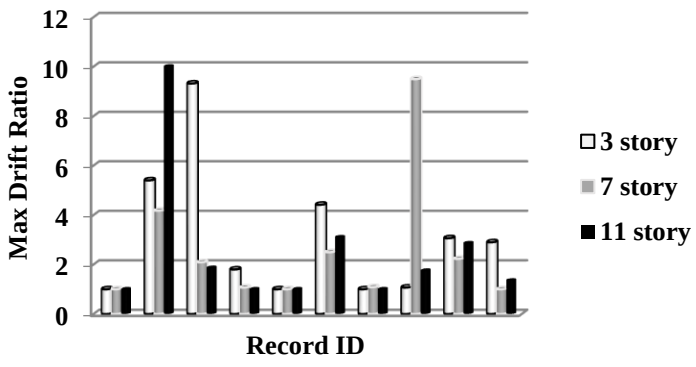

Fig. 16. Maximum Roof drift ratio for CBFs with 3, 7 and 11 story.

6.4. Sensitivity of the seismic demand parameters with ANN

As mentioned in the previous sections, this paper is dedicated to evaluate the variation of seismic demand parameters such as R factor, maximum roof drift ratio and damage index ratio of CBFs under critical successive earthquakes. In this regard, artificial neural networks with two hidden layers are used to estimate the target values. This ideal neural network with the optimal number of nodes in hidden layers is achieved by designing many networks with a different number of nodes in each hidden layer and selecting the best network with the highest correlation coefficient R and the lowest error rate. The optimal number of nodes in the hidden layers is found to be 11 and 13 in the present research. This network is able to estimate each of the three above-mentioned parameters simultaneously by defining the target ID (equal to 1 for $R_{sequence}$, 2 for $DI_{sequence/single}$ and 3 for $MD_{sequence/single}$). So that, the correlations between the outputs and the target values in training, testing, and validation steps are 97%, 98% and 95%. As shown in Fig 17, the correlation coefficient R is close to 1 and is followed by a perfect correlation between the neural network outputs and the target values, resulting in a very low error rate.

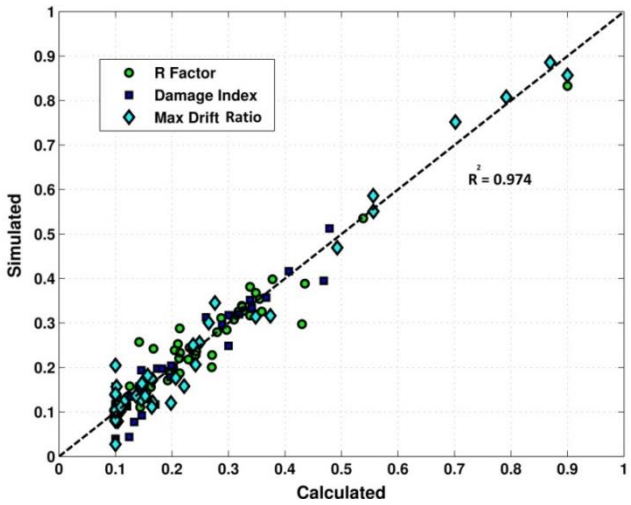

Fig. 17. Comparison of estimated results by ideal neural network with real values in normal case.

Next, sensitivity of the reduced behavior factor increased the damage index, and the maximum drift of CBFs, caused by critical consecutive earthquakes, is evaluated using the ideal neural network designed in the previous step. In this regard, variation of the desired parameters is investigated with T, PGA_a and PGA_m. In the first step, all inputs - except T - are considered equal to the average values introduced in Table 3. Ideal ANN estimates the reduced R factor and increased damage index for different values of period, as presented in Fig 18. The empirical Equations (4) and (5) are proposed to formulate these variations:

$$R = 2.722e^{-6.608T} + 0.002452e^{7.124T} \quad (4)$$

$$DI = 5.9026T^2 - 3.7474T + 0.7902 \quad (5)$$

Since the use of artificial successive earthquakes as seismic scenarios can cause unrealistic results, the effect of repeated shocks as “Back to back or B2B” is examined on the reduced R factor and increased damage index. For this purpose, the first shock is used as a second shock, and PGA_a is presented equal to PGA_m to ANN. Despite the assumptions of seismic design codes, Fig. 18 shows R factors are not constant for CBFs with different heights. Therefore, structural designs using a constant behavior factor can lead to non-conservative results. Moreover, CBFs have different

performances under real and back to back scenarios, so structural damage caused by artificial successive shocks is less than real damages. This difference presented in Fig 19 highlights the necessity of seismic sequence phenomenon in the structural design procedure, especially for taller buildings. In the next step, variation of the maximum drift ratio (MD) with 1st shock PGA (PGA_m) is evaluated for different types of CBFs, which have been considered using various periods in Fig 20. As shown in this figure, taller CBFs undergo more drifts under a desired earthquake with specific PGA.

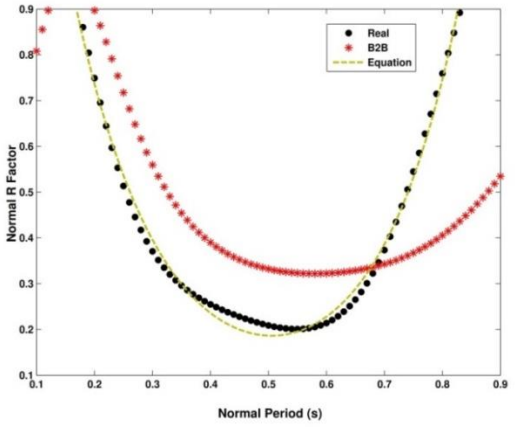

(a)

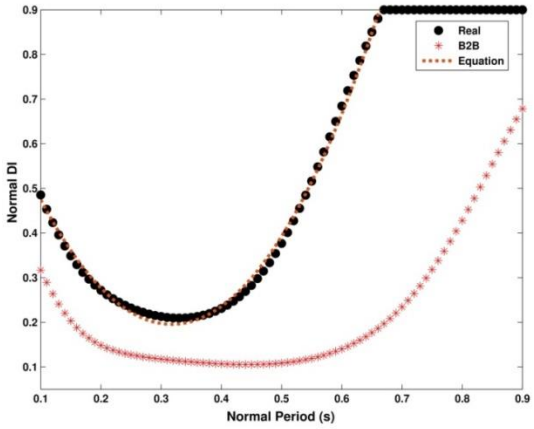

(b)

Fig. 18. Variation of (a) Reduced R factors, (b) Increased damage index with periods.

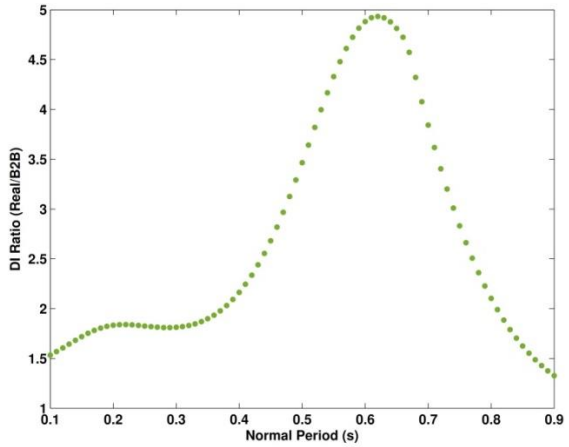

Fig. 19. Comparison between increased damage under real to artificial successive records.

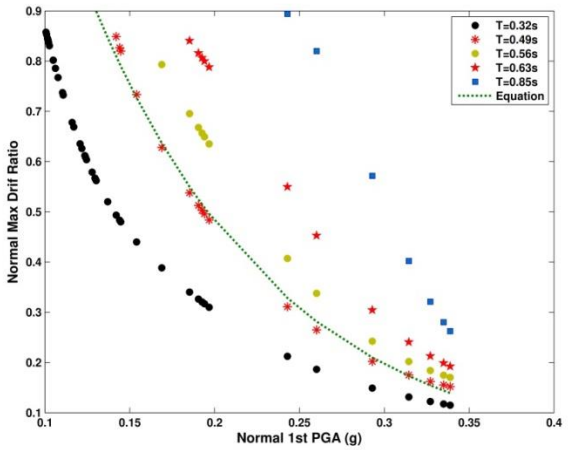

Fig. 20 Maximum drift ratios for various CBFs under successive earthquakes with different PGA_m.

In successive scenarios, if the first shock has a lower PGA rather than next shock, the MD will be increased because of a stronger second shock. Taller CBFs will be affected more than others. Equation (6) presents the variation of MD with PGA_m:

$$MD = 2.8858e^{-8.948PGA_m} \tag{6}$$

In completing the above results, sensitivity of MD to the second shock PGA (PGA_a) is evaluated for various ranges of CBFs – distinguished from several periods – under successive earthquakes with different PGA_a in the last step. Successive earthquakes with stronger 2nd shock, in comparison with 1st shock, have a more significant effect on the MD of CBFs. This effect is shown in Fig. 21 and formulated in Equation (7). As shown in this figure, taller CBFs are more affected under specific scenario. As the PGA_a is increased, CBFs undergo more MD at the end of the successive scenario.

$$MD = 0.08917e^{1.641PGA_a} + 1.053e - 5e^{45.93PGA_a} \tag{7}$$

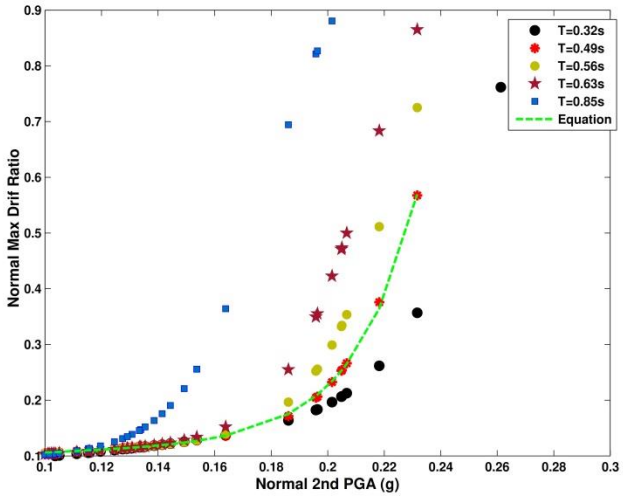

Fig. 21. Maximum drift ratio for various CBFs under successive earthquakes with different PGA_a.

8. Conclusions

This paper evaluates the seismic demand parameters such as behavior factor, displacement amplification factor (C_d), maximum drift and damage index (DI) of special steel chevron-braced frames under critical single and consecutive seismic scenarios and estimate the sensitivity of these

factors using an ideal artificial neural network. In this way, three frames with 3, 7, and 11 stories are designed and analyzed under 15 records containing critical single and consecutive earthquakes as the mainshock with foreshock and aftershock with a time interval of 100 seconds. In this regard, nonlinear dynamic analysis, pushover, linear dynamic analysis and incremental dynamic analysis are performed on CBFs. Firstly, the ductility, over-strength, and behavior factors are calculated based on [31] by calculating the maximum linear and nonlinear base shear and the base shear of the first plastic hinge. In the following, increased structural damage due to accumulation damages caused by previously shocks is determined based on Park and Ang (1985) damage index. Then, C_d ratio and maximum roof drift are determined for all CBFs under critical scenarios with/without successive shocks. Finally, the ideal artificial neural network using structural features, first earthquake, and second earthquake, and the above-mentioned results which have been obtained from the analyses' results are designed, trained, and validated to estimate the sensitivity of seismic demand parameters under critical successive earthquakes. The main conclusions from this paper are as follows:

- Based on the results of IDA curves, the collapse capacity of CBFs with 3, 7 and 11-storey is decreased due to the accumulation of damage caused by the first earthquake in the elements with strength deterioration. The damaged structures collapse under successive earthquakes much sooner than what is assumed in the design codes by considering the individual earthquake.
- The results of this paper show a reduction rate for behavior factors (about 14%), incremental rate for damage index (1.8 times) and slight changes for C_d (not significantly) due to incidence of critical successive shocks.
- Since the calculation of seismic demand parameters is a time-consuming process and the number of studied CBFs is limited, artificial neural network is a good technique for estimating these factors for more states. In this paper, a feed-forward neural network with two hidden layers containing 11 and 13 nodes in the first and second layers estimates the seismic demand parameters for CBFs under critical successive earthquakes simultaneously with minor error. This network which has good performance, can estimate seismic demand parameters with sufficient accuracy and evaluate the sensitivity of these parameters to structural and seismic excitation features.
- Although, the use of artificial successive earthquakes – for example back to back method which considers similar time history for first and second shock – may be better than considering only single records, realistic performance of structures depends on the real consecutive earthquakes.
- Since that Iran country is located in high risk seismic zone, it is essential to study the seismic sequence phenomenon and its effect on structures' behavior, especially structures whose performance is important after the earthquake. Due to the short time interval between two shocks, most of the time, there is no opportunity to repair the structure and the damaged structure exposed to the first earthquake, in the face of the next strong earthquakes suffers more severe damages.
- Despite the importance of the seismic sequence phenomenon, there are no criteria for considering this phenomenon in design regulations such as the Iranian Standard of 2800. Only a single earthquake is considered in the design of the structure, and there is no difference between the performance of the structure under single and successive

earthquakes. In that case, the structure may not respond to successive earthquakes' resulting demands and suffer more damages and even collapse.

- According to the results of sensitivity analysis, R factor is usually changed with seismic excitation features. Therefore, despite what is necessitated in the seismic design codes, proposing a constant value as R factor for whole steel structure cannot lead to proper design of structures.

Funding

This research did not receive any specific grant from funding agencies in the public, commercial, or not-for-profit sectors.

Conflicts of interest

The authors declare that they have no known competing financial interests or personal relationships that could have appeared to influence the work reported in this paper.

Authors contribution statement

Sahar Rouzrokh: Conceptualization, Investigation, Roles/Writing – original draft, Project administration, Visualization.

Elham Rajabi: Data curation, Formal analysis, Investigation, Methodology, Roles/Writing – original draft, Project administration.

Gholamreza Ghodrati Amiri: Conceptualization, Investigation, Project administration, Visualization**,** Supervision**.**

References

[1] Gautam D, Rodrigues H, Bhetwal KK, Neupane P, Sanada Y. Common structural and construction deficiencies of Nepalese buildings. Innov Infrastruct Solut 2016;1. doi:10.1007/s41062-016-0001-3.

[2] Rajabi ES-S of R and SF under CM-AGM, Amiri GG. Damage Sensitive-Stories of RC and Steel Frames under Critical Mainshock-Aftershock Ground Motions. J Rehabil Civ Eng 2022;10. doi:10.22075/JRCE.2021.22564.1487.

[3] Pu W, Li Y. Evaluating structural failure probability during aftershocks based on spatiotemporal simulation of the regional earthquake sequence. Eng Struct 2023;275. doi:10.1016/j.engstruct.2022.115267.

[4] Ke K, Zhou X, Zhu M, Yam MCH, Zhang H. Seismic demand amplification of steel frames with SMAs induced by earthquake sequences. J Constr Steel Res 2023;207. doi:10.1016/j.jcsr.2023.107929.

[5] Fang C, Ping B, Zheng Y, Ping Y, Ling H. Seismic fragility and loss estimation of self-centering steel braced frames under mainshock-aftershock sequences. J Build Eng 2023;73. doi:10.1016/j.jobe.2023.106433.

[6] Narayan S, Shrimali MK, Bharti SD, Datta TK. Effects of aftershocks on the performance of steel building frames. Structures 2023;56. doi:10.1016/j.istruc.2023.104959.

[7] Hoveidae N, Radpour S. Performance evaluation of buckling-restrained braced frames under repeated earthquakes. Bull Earthq Eng 2021;19. doi:10.1007/s10518-020-00983-0.

[8] Goda K, Taylor CA. Effects of aftershocks on peak ductility demand due to strong ground motion records from shallow crustal earthquakes. Earthq Eng Struct Dyn 2012;41. doi:10.1002/eqe.2188.

[9] Veismoradi S, Cheraghi A, Darvishan E. Probabilistic mainshock-aftershock collapse risk assessment of buckling restrained braced frames. Soil Dyn Earthq Eng 2018;115. doi:10.1016/j.soildyn.2018.08.029.

[10] Banayan-Kermani A, Bargi K. Seismic collapse assessment of intermediate RC moment frames subjected to mainshock-aftershock sequences. Results Eng 2023;20. doi:10.1016/j.rineng.2023.101629.

[11] Kouhestanian H, Razmkhah MH, Shafaei J, Pahlavan H, Shamekhi Amiri M. Probabilistic Evaluation of Seismic Performance of Steel Buildings with Torsional Irregularities in Plan and Soft Story under Mainshock-Aftershock Sequence. Shock Vib 2023;2023. doi:10.1155/2023/9549121.

[12] Andalib Z, Ali Kafi M, Bazzaz M, Momenzadeh S. Numerical evaluation of ductility and energy absorption of steel rings constructed from plates. Eng Struct 2018;169. doi:10.1016/j.engstruct.2018.05.034.

[13] Bazzaz M, Andalib Z, Kheyroddin A, Kafi MA. Numerical comparison of the seismic performance of steel rings in off-centre bracing system and diagonal bracing system. Steel Compos Struct 2015;19. doi:10.12989/scs.2015.19.4.917.

[14] Bazzaz M, Andalib Z, Kafi MA, Kheyroddin A. Evaluating the performance of OBS-C-O in steel frames under monotonic load. Earthq Struct 2015;8. doi:10.12989/eas.2015.8.3.699.

[15] Andalib Z, Kafi MA, Kheyroddin A, Bazzaz M. Experimental investigation of the ductility and performance of steel rings constructed from plates. J Constr Steel Res 2014;103. doi:10.1016/j.jcsr.2014.07.016.

[16] Bazzaz M, Kafi MA, Kheyroddin A, Andalib Z, Esmaeili H. Evaluating the seismic performance of off-centre bracing system with circular element in optimum place. Int J Steel Struct 2014;14. doi:10.1007/s13296-014-2009-x.

[17] Bazzaz M, Kheyroddin A, Kafi MA, Andalib Z. Evaluation of the seismic performance of off-centre bracing system with ductile element in steel frames. Steel Compos Struct 2012;12. doi:10.12989/scs.2012.12.5.445.

[18] Loulelis D, Hatzigeorgiou GD, Beskos DE. Moment resisting steel frames under repeated earthquakes. Earthq Struct 2012;3. doi:10.12989/eas.2012.3.3_4.231.

[19] Shokrabadi M, Burton H V. Building service life economic loss assessment under sequential seismic events. Earthq Eng Struct Dyn 2018;47. doi:10.1002/eqe.3045.

[20] Hu J, Wen W, Zhai C, Pei S, Ji D. Seismic resilience assessment of buildings considering the effects of mainshock and multiple aftershocks. J Build Eng 2023;68. doi:10.1016/j.jobe.2023.106110.

[21] Ghaderi M, Gholizadeh S. Mainshock–aftershock low-cycle fatigue damage evaluation of performance-based optimally designed steel moment frames. Eng Struct Low-Cycle Fatigue Damage Eval Performance-Based Optim Des Steel Moment Fram 2021;237. doi:10.1016/j.engstruct.2021.112207.

[22] Rajabi E, Golestani Y. Study of steel buildings with LCF system under critical mainshock-aftershock sequence: Evaluation of fragility curves and estimation of the response modification factor by artificial intelligence. Structures 2023;56. doi:10.1016/j.istruc.2023.105044.

[23] Rajabi E, Ghodrati Amiri G. Behavior factor prediction equations for reinforced concrete frames under critical mainshock-aftershock sequences using artificial neural networks. Sustain Resilient Infrastruct 2022;7. doi:10.1080/23789689.2021.1970301.

[24] Abdollahzadeh G, Sadeghi A. Earthquake recurrence effect on the response reduction factor of steel moment frame. Asian J Civ Eng 2018;19. doi:10.1007/s42107-018-0079-3.

[25] Amiri GG, Dana FM. Introduction of the most suitable parameter for selection of critical earthquake. Comput Struct 2005;83. doi:10.1016/j.compstruc.2004.10.010.

[26] Hatzigeorgiou GD. Behavior factors for nonlinear structures subjected to multiple near-fault earthquakes. Comput Struct 2010;88. doi:10.1016/j.compstruc.2009.11.006.

[27] Gholhaki M, Pachideh G, Lashkari R, Rezayfar O. Behaviour of buckling-restrained brace equipped with steel and polyamide casing. Proc Inst Civ Eng Struct Build 2021;174. doi:10.1680/jstbu.19.00206.

[28] Pachideh G, Gholhaki M, Kafi M. Experimental and numerical evaluation of an innovative diamond-scheme bracing system equipped with a yielding damper. Steel Compos Struct 2020;36. doi:10.12989/scs.2020.36.2.197.

[29] Deierlein GG, Reinhorn AM, Willford MR. Nonlinear Structural Analysis For Seismic Design: A Guide for Practicing Engineers. Design 2010.

[30] Kim J, Choi H. Response modification factors of chevron-braced frames. Eng Struct 2005;27. doi:10.1016/j.engstruct.2004.10.009.

[31] Uang C. Establishing R (or Rw) and Cd Factors for Building Seismic Provisions. J Struct Eng 1991;117:19–28. doi:10.1061/(ASCE)0733-9445(1991)117:1(19).

[32] Park Y, Ang AH -S. Mechanistic Seismic Damage Model for Reinforced Concrete. J Struct Eng 1985;111. doi:10.1061/(asce)0733-9445(1985)111:4(722).

[33] Hait P, Sil A, Choudhury S. Damage assessment of low to mid rise reinforced concrete buildings considering planner irregularities. Int J Comput Methods Eng Sci Mech 2020;22. doi:10.1080/15502287.2020.1856971.

[34] Pachideh G, Gholhaki M, Saedi Daryan A. Analyzing the damage index of steel plate shear walls using pushover analysis. Structures 2019;20. doi:10.1016/j.istruc.2019.05.005.

[35] Maulana TI, Enkhtengis B, Saito T. Proposal of damage index ratio for low-to mid-rise reinforced concrete moment-resisting frame with setback subjected to uniaxial seismic loading. Appl Sci 2021;11. doi:10.3390/app11156754.

[36] Lakhade SO, Kumar R, Jaiswal OR. Estimation of drift limits for different seismic damage states of RC frame staging in elevated water tanks using Park and Ang damage index. Earthq Eng Eng Vib 2020;19. doi:10.1007/s11803-020-0554-1.

[37] Carrillo J, Oyarzo-Vera C, Blandón C. Damage assessment of squat, thin and lightly-reinforced concrete walls by the Park & Ang damage index. J Build Eng 2019;26. doi:10.1016/j.jobe.2019.100921.

[38] Chen Z, Li X, Wang W, Li Y, Shi L, Li Y. Residual strength prediction of corroded pipelines using multilayer perceptron and modified feedforward neural network. Reliab Eng Syst Saf 2023;231. doi:10.1016/j.ress.2022.108980.

[39] Rastin Z, Ghodrati Amiri G, Darvishan E. Generative Adversarial Network for Damage Identification in Civil Structures. Shock Vib 2021;2021. doi:10.1155/2021/3987835.

[40] Zhang X, Li ZX, Shi Y, Wu C, Li J. Fragility analysis for performance-based blast design of FRP-strengthened RC columns using artificial neural network. J Build Eng 2022;52. doi:10.1016/j.jobe.2022.104364.

[41] Leung CK, Ng MY, Luk HC. Empirical Approach for Determining Ultimate FRP Strain in FRP-Strengthened Concrete Beams. J Compos Constr 2006;10. doi:10.1061/(asce)1090-0268(2006)10:2(125).

[42] Vamvatsikos D, Cornell CA. Incremental dynamic analysis. Earthq Eng Struct Dyn 2002;31:491–514. doi:10.1002/eqe.141.

[43] FEMA. Multi-hazard loss estimation methodology, earthquake model, 1. HAZUS-MH2.1. Dep Homel Secur Fed Emerg Manag Agency Mitig Div Washington, DC 2013.

[44] Atkinson GM. Earthquake time histories compatible with the 2005 NBCC Uniform Hazard Spectrum. Can J Civ Eng 2009;36.